RASĀYAN *J. Chem.*
Vol. 19 | No. 3 | 1482-1488 | July-September | 2026
ISSN: 0974-1496 | e-ISSN: 0976-0083 | CODEN: RJCABP
http://www.rasayanjournal.com
http://www.rasayanjournal.co.in

SUNLIGHT-ACTIVE MESOPOROUS Zn-TiO_2 QUASI-SPHERES FOR ENHANCED DECOLORIZATION OF DISTILLERY SPENT WASH

A. S. Bhosale[1,✉], N. P. Mali[1], S. B. Dhotre[1], S. P. Takle[1], A. S. Ware[2], D. B. Bankar[3], R. U. Mene[4], and N. N. Bhujbal[1]

[1]Department of Chemistry, PDEA's Annasaheb Magar Mahavidyalaya, Hadapsar, Pune-411028, Maharashtra, India

[2]MAEER'S MIT Saint Dnyaneshwar College, Pune-412105, Maharashtra, India

[3]P.G. Department of Chemistry, R. B. Narayanrao Borawake College, Shrirampur-413709, Maharashtra, India

[4]Department of Physics, PDEA's Annasaheb Magar Mahavidyalaya, Hadapsar, Pune-411028, Maharashtra, India

✉Corresponding author: amolbhosale4141@gmail.com

ABSTRACT

Sugarcane-based distillery spent wash is a notoriously challenging malodorous effluent, characterised by its acidic pH, intense dark brown colour, and high organic load. These features seriously harm the aquatic ecosystem and environmental sustainability. In this paper, Zn-TiO_2 nanocatalysts with 1-5 wt.% Zn were synthesized by using the hydrothermal method. A systematic study of the structural features, optical response and photocatalytic properties of TiO_2 was conducted to evaluate the influence of Zn doping. Characterisation of the catalysts was carried out using X-ray diffraction, FESEM, TEM, Raman analysis, UV–DRS, and BET techniques. Zn-doped TiO_2 exhibited a quasi-spherical morphology with particle size ranging from 10 to 25 nm. Doping results in a shift of Raman peaks toward lower wavenumbers and causes the band gap energy to decline from 3.03 eV to 2.8 eV. Photocatalytic performance under solar light was investigated by monitoring decolourisation efficiency and the extent of COD and TOC reduction of the spent wash. Among all doped samples, the 3% Zn-TiO_2 sample exhibits higher photocatalytic activity (84%) compared to undoped TiO_2 (64%) under the same conditions. These findings demonstrate the potential of Zn–TiO_2 as an efficient photocatalyst for sustainable wastewater treatment.

Keywords: Spent Wash, Distillery, Photocatalyst, Degradation, Hydrothermal, Sustainability.

RASĀYAN *J. Chem.*, Vol. 19, No.3, 2026

INTRODUCTION

Availability of clean water is essential for both human civilisation and the maintenance of ecological balance. Freshwater reserves around the world are under stress due to industrial development and population growth, which turns severe water scarcity in many regions of the globe.[1] This study supports global efforts to improve water quality through environmentally friendly wastewater treatment. The distillery industry is one of the leading contributors to water pollution and generates huge amounts of high-strength wastewater during the production of alcohol.[2] It has been estimated that 12-15 litres of spent wash are generated for every litre of ethanol produced.[3] Distillery spent wash is characterised by intense colour with high concentrations of total dissolved solids (TDS), acidic pH and a complex mixture of contaminants.[4] A characteristics dark brown colour of distillery spent wash, primarily attributed to the presence of melanoidin polymers.[5] The problematic feature of melanoidin is its resistance to microbial degradation.[6] Because of these limitations, the conventional treatment strategies rarely achieve complete degradation of the complex, colour-forming organic compounds present in spent wash. Therefore, advanced oxidation processes (AOPs) have drawn growing interest in recent years.[7] These methods involve the in situ formation of highly reactive species, especially hydroxyl radicals, which are capable of attacking and breaking down otherwise persistent organic molecules.[8] Unlike many traditional treatments, AOPs can handle non-biodegradable and recalcitrant pollutants more effectively.[9] Among the various

AOPs, semiconductor photocatalysis is considered a promising and environmentally friendly approach, leading to complete mineralisation of pollutants under light irradiation without producing problematic secondary waste.[10–12] Titanium dioxide has been widely explored as a fundamental material in photocatalytic studies for many years. Due to its stability, affordability, low toxicity and strong oxidative ability make it an attractive photocatalyst, and it has already shown promising results in the degradation of dyes, pesticides and other organic contaminants.[13–17] At the same time, the practical deployment of undoped TiO_2 is limited. The wide band gap limits photoactivity mainly in the UV region, which accounts for only a minor portion of the solar spectrum. In addition, its overall efficiency is reduced due to rapid photogenerated charge carrier recombination.[18–20] To enhance the visible-light utilisation efficiency of TiO_2, several modification strategies have been proposed over the years.[21] Among various transition-metal dopants, Zinc is considered a suitable dopant. Zn doping modifies the TiO_2 band structure by introducing new energy levels, facilitating better charge separation and visible-light absorption.[22,23] Various synthesis techniques have been employed for the preparation of transition metal-doped TiO_2 nanomaterials.

The hydrothermally synthesised materials generally show improved crystallinity, controlled morphology and reduced structural defects. But, limited studies are available on Zn-doped TiO_2 synthesised via the hydrothermal method for the treatment of distillery wastewater. Hence, systematic investigation using spent wash is necessary, particularly under natural sunlight conditions for real wastewater treatment applications. This work presents a hydrothermally synthesised, optimally Zn-doped TiO_2 photocatalyst that combines high solar-driven activity, mechanistic understanding and practical applicability for real industrial wastewater, offering a superior improvement over existing catalysts in terms of performance, sustainability and scalability.

EXPERIMENTAL

Material

The Chemicals for the synthesis are Titanium (IV) tetraisopropoxide (TTIP), received from Sigma Aldrich, 30% w/w Hydrogen Peroxide (H_2O_2) from Merck India Ltd, and Zinc nitrate hexahydrate from Merck India Ltd, which were used without further purification.

Synthesis of Catalyst

A hydrothermal technique was utilised for the preparation of undoped and Zn-doped TiO_2 nanoparticles. For Zn-doped titania, A 3.4 mL of Titanium Isopropoxide was hydrolysed by using 100 mL Millipore water with stirring at 500 rpm for 1 hr. to get a white precipitate of titanium hydroxide. Keep this solution without disturbing for some time to allow a white precipitate to settle down. The supernatant liquid removed by decantation contains alcohol left after the hydrolysis of TTIP. To this amorphous precipitate a 30 mL of 30% H_2O_2 was added to dissolve the precipitate to form an orange colour sol with stirring.

The zinc nitrate hexahydrate (1-5 wt.%) was dissolved in hydrogen peroxide and water to get a clear solution, and was added to the above solution. After some time, the sol is converted into a viscous gel. Place this gel with 80 mL Millipore water into the teflon-lined autoclave and heat in the oven at 150℃ for 12 hr. The product obtained from the autoclave is thoroughly washed using Millipore water and oven-dried at 105℃ to get dried Zn-doped TiO_2 powder. For the synthesis of undoped TiO_2 nanoparticles, the same procedure was followed without adding zinc nitrate hexahydrate.

Characterization

X-ray diffraction analysis was performed to investigate the phase structure and crystallite size of the nanomaterials, employing Cu Kα radiation (λ = 1.5418 Å) on a Rigaku D-MAX/A9 instrument. Detailed analysis of the catalyst's morphology, size and microstructural characteristics was performed using TEM and FESEM techniques with JEOL 2100F and Thermo Fisher Scios 2 instruments, respectively. UV–Visible diffuse reflectance spectrometer was used over the 250 to 750 nm range on a Perkin Elmer spectrophotometer to estimate the band gap energies. BET measurements were conducted with a Quantachrome Nova 2200 instrument to evaluate the surface area of the samples. A HORIBA Scientific Raman spectrophotometer was used to analyse the Raman shift due to doping.

RESULTS AND DISCUSSION

XRD Analysis

The crystal structures of hydrothermally synthesised catalysts at 120°C, 150°C and 180°C were examined using X-ray diffraction (XRD). Figure-1(a-c) shows the corresponding diffraction patterns, with curve (a) representing the sample synthesised at 120°C. Suggesting that anatase is the dominant phase at this temperature. Upon increasing the synthesis temperature to 150°C (curve b), the anatase peaks become noticeably more intense. This change likely reflects improved crystallinity rather than a phase change, as no additional reflections appear. At 180°C (curve c), the diffraction peaks sharpen further and show higher intensity, pointing to enhanced crystal growth. This subtle feature suggests that while anatase remains dominant, the onset of anatase-to-rutile transformation may begin near 180°C rather than occurring abruptly. Since the anatase TiO_2 is generally considered more effective for photocatalytic degradation, all Zn-doped TiO_2 catalysts (1-5 wt.%) were synthesised at 150°C to retain phase purity while achieving reasonable crystallinity. The calculated particle sizes range from 8 to 20 nm for all samples. Broadening of diffraction peaks is observed in the Zn-doped sample throughout, which typically points to small crystallite dimensions and the presence of lattice imperfections. These structural characteristics are beneficial for photocatalytic applications, as they enhance surface reactivity and improve charge carrier dynamics.

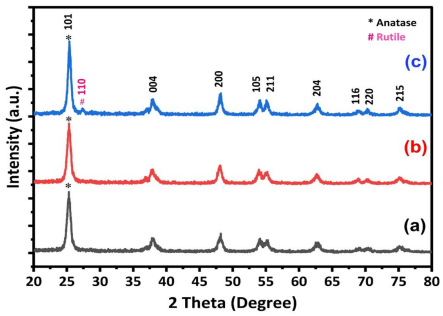

Fig.-1: X-Ray Diffraction Patterns of 1% Zn–TiO_2 Synthesized by the Hydrothermal Method at (a) 120℃, (b) 150℃ and (c) 180℃ for 12 hr

FE-SEM and TEM Analysis

The morphological features, particle size and elemental composition of undoped and Zn-doped TiO_2 nanoparticles were analysed using field emission scanning electron microscopy (FESEM) and high-resolution transmission electron microscopy (HRTEM). As illustrated in Fig.-2, the particles appear quasi-spherical and fairly well dispersed, with a size in the range of 10-25 nm. Zn doping results in reduced agglomeration, improved particle uniformity and a porous surface structure. No secondary phases are visible in these images, which suggests that Zn is well incorporated rather than forming separate oxide particles. This uniform incorporation contributes to improved catalytic efficiency by increasing the availability of active sites. The high-resolution image Fig.-2(e) reveals clear and well-defined lattice fringes, pointing to the crystallinity of the material. An interplanar spacing of approximately 0.35 nm was observed, which is in good agreement with the (101) lattice plane of the anatase structure of TiO_2. The SAED image presented in Fig.-2(f) reveals a sharp concentric diffraction ring, a typical signature of polycrystalline materials.

Raman Spectra of Zn-TiO_2

The modification of the TiO_2 lattice due to Zn doping was examined through Raman spectroscopy. The Raman spectra of both undoped and Zn-TiO_2 samples are presented in Fig.-3. For undoped TiO_2, the main mode appears at about 144.6 cm^{-1}, but in the case of 3% Zn-TiO_2, the corresponding Raman bands shift slightly to higher wavenumbers around 146.4 cm^{-1}. No additional peaks related to metallic Zn or zinc oxide phases are detected, which suggests that Zn is incorporated into the TiO_2 structure rather than forming a separate phase. A clear change is seen after Zn incorporation. These shifts and peak broadenings likely reflect local lattice distortions caused by Zn^{2+} ions substituting for Ti^{4+}. This confirms the successful incorporation of Zn into the TiO_2 lattice without forming secondary phases.

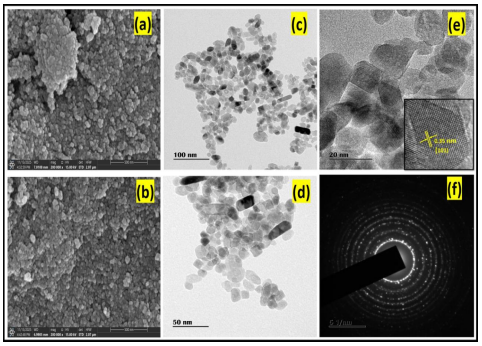

Fig.-2: FESEM Image of (a) TiO_2, (b) 3% Zn–TiO_2 and HRTEM images (c) and (d) low-magnification, (e) High-Magnification (inset: lattice fringes) and (f) SAED Pattern of 3% Zn–TiO_2 Synthesised at 150℃ for 12 hr

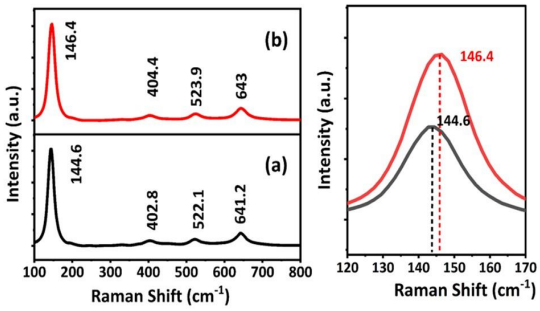

Fig.-3: Raman Spectra of (a) Undoped TiO_2, (b) 3% Zn-TiO_2 Sample and (c) Raman Shift of the Main Intense Peak

UV DRS Study

The UV-visible absorption spectra of undoped and Zn-doped TiO_2 samples with varying Zn content are depicted in Fig.-4. The spectra of undoped TiO_2 exhibit a distinct absorption edge in the ultraviolet region, reflecting its broad energy band gap feature. In the Zn-TiO_2 Sample, the absorption edge shifts toward longer wavelengths. This bathochromic shift becomes more noticeable as the Zn concentration rises, suggesting changes in the electronic framework of TiO_2 caused by Zn incorporation, where Zn-induced defect levels and oxygen vacancies contribute to band gap narrowing. Optical band gap estimation was performed using Tauc analysis by plotting $(\alpha h\nu)^2$ against photon energy, as indicated in the inset of Fig.-4. Undoped TiO_2 exhibits the largest band gap value, 3.03 eV, while the Zn-doped samples show a gradual reduction in band gap to about 2.8 eV with increasing Zn content. This band gap reduction enhances visible light absorption under solar irradiation.

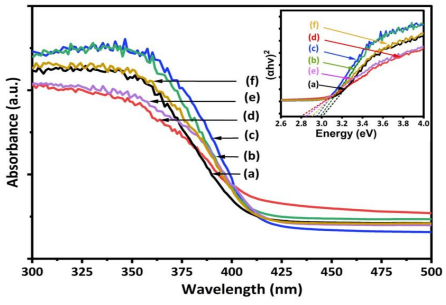

Fig.-4: UV-Visible DRS Spectra of Samples Synthesised at 150℃ (a) TiO_2, (b) 1% Zn-TiO_2, (c) 2% Zn-TiO_2, (d) 3% Zn-TiO_2, (e) 4% Zn-TiO_2 and (f) 5% Zn-TiO_2. Inset is the Tauc Plot of (a) TiO_2 and (b-f) 1-5 wt.% of Zn-doped TiO_2

BET Surface Area Analysis

The porosity and surface area of the catalysts were investigated using N_2 physisorption along with BET analysis. As presented in Fig.-5, the Zn-doped sample exhibits a type IV N_2 adsorption–desorption isotherm with an H2-type hysteresis loop. For undoped TiO_2 calcined at 400 °C, the measured surface area was around 84 m^2/g, having a pore volume of 0.15 cm^3/g. The Zn–TiO_2 samples show a higher

surface area, reaching about 120.55 m^2/g, along with an improved pore volume of 0.22 cm^3/g. The observed increase in surface area and pore volume upon Zn doping is attributed to the role of Zn ions in suppressing particle growth during calcination, resulting in a more open mesoporous structure that facilitates mass transport during photocatalysis.

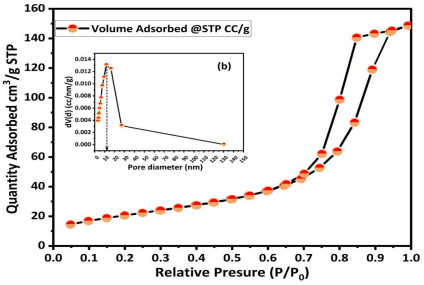

Fig.-5: N_2 Adsorption and Desorption Isotherm of (a) 3% Zn-TiO_2 Synthesised at 150℃ for 12 hr. Inset (b) BJH Adsorption Pore Size Distribution Curve

Photocatalytic Performance

The photocatalytic performance of undoped and Zn-doped TiO_2 catalyst (1–5 wt.%) was evaluated using sugarcane distillery raw spent wash as the target pollutant. For all experiments, the spent wash concentration was fixed at 2500 ppm. All photocatalytic experiments were carried out under natural solar irradiation. To establish a baseline, photolysis experiments were performed without any catalyst. Under these conditions, colour and COD reduction were minimal (only ~2.7% and 1.6%, respectively), suggesting that direct sunlight alone is largely ineffective for treating spent wash. The progress of degradation was tracked by periodically measuring colour intensity and pollutant concentration using UV–visible spectroscopic analysis. The UV–visible spectra of spent wash treated with undoped and 3% Zn-doped TiO_2 at different irradiation times are presented in Fig.-6(A) and (B). The variation of percentage degradation with irradiation time for TiO_2 and Zn–TiO_2 catalysts is shown in Fig.-6 (C). Under solar irradiation, undoped TiO_2 achieved about 64% color reduction, along with noticeable reductions in COD (~540 ppm) and TOC (~204 ppm). In contrast, Zn doping led to a clear improvement in photocatalytic performance. As the Zn content increased from 1% to 3%, both colour intensity and organic load decreased more rapidly. Among the tested catalysts, 3% Zn–TiO_2 appeared to be the most effective, reaching approximately 84% decolorization and reducing COD and TOC to around 270 ppm and 102 ppm, respectively. Interestingly, increasing the Zn content beyond 3% led to a slight drop in efficiency. The 4% and 5% Zn–TiO_2 samples showed lower colour reduction (about 81% and 78%) and relatively higher residual COD and TOC values. To better understand the degradation behavior, the reaction kinetics were examined using the Langmuir–Hinshelwood pseudo–first-order approach.

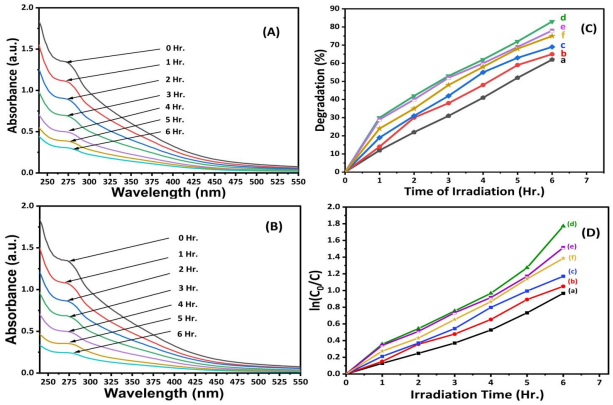

Fig.-6: UV–Vis Absorbance Spectra of (A) Undoped TiO_2, (B) 3% Zn Doped TiO_2 and (C) and (D) is Percentage Degradation and Degradation Rate of (a) TiO_2, (b) 1% Zn-TiO_2, (c) 2% Zn-TiO_2, (d) 3% Zn-TiO_2, (e) 4% Zn-TiO_2 and (f) 5% Zn-TiO_2 respectively Under Natural Sunlight

As illustrated in Fig. 6(D), the graph of $\ln(C_0/C_t)$ against exposure time exhibited excellent linearity, yielding R^2 values greater than 0.98 for every catalyst. The 3% Zn–TiO_2 sample also exhibited the highest

reaction rate constant (k=0.0200 min^{-1}). A similar trend was observed in reaction kinetics, where the apparent rate constant increased up to 3% Zn loading. Beyond this level, a slight decrease in rate constant was observed for the 4% and 5% Zn–TiO_2 samples. The reusability and stability of the optimized 3% Zn–TiO_2 photocatalyst were assessed by four repetitive photocatalytic degradation cycles of distillery spent wash under the same experimental conditions. The fresh catalyst showed the best activity in the first cycle, maintaining high degradation efficiency. Even after four consecutive cycles, the catalyst was still able to remove about 78% of the colour and about 68% of the COD.

CONCLUSION

In this study, undoped and Zn-doped TiO_2 was successfully synthesised by using the hydrothermal method. Upon doping with Zn, the photocatalytic activity of the catalyst is enhanced by decreasing crystalline size, reducing the band gap and increasing the surface area. The particle size of the material is analysed by using FESEM, which ranges from 10-25 nm. A slight agglomeration of particles was observed in both the doped and undoped samples. Upon incorporation of Zn, the band gap narrows from 3.03 to 2.80 eV, improving light absorption. BET surface area analysis confirms the notable increase in surface area after Zn insertion. Among all sample 3% Zn-TiO_2 exhibit superior photocatalytic activity, achieving 84% degradation of spent wash colour, while pristine TiO_2 shows about 64% of degradation. 3% Zn-TiO_2 shows excellent stability and reusability, retaining about 90% of its initial degradation efficiency after 4 cycles. These results indicate that hydrothermally synthesised Zn-TiO_2 is a sustainable photocatalyst for treating distillery spent wash under solar irradiation, due to its high efficiency, reusability and utilisation of sunlight as a clean energy source. This catalyst reveals strong potential for large-scale deployment in industrial wastewater treatment systems, offering a reliable pathway for practical and sustainable environmental remediation.

ACKNOWLEDGMENTS

The author sincerely thanks Dr. Namdeo Bhujbal and Dr. Ravindra Mene for their valuable guidance and continuous support. The author also acknowledges Dr. Shrikant Takle and Dr. Aarti Ware for helpful discussions. Gratitude is extended to the Department of Chemistry, Annasaheb Magar Mahavidyalay, Hadapsar, Pune and Vidya Pratishthan's Supe Arts, Science and Commerce College, Supe, Baramati, Pune, for providing laboratory facilities.

CONFLICT OF INTERESTS

The authors declare that there is no conflict of interest.

AUTHOR CONTRIBUTIONS

The present work is related to *SDG-6: Clean Water and Sanitation*. All the authors contributed significantly to this manuscript, participated in reviewing/editing and approved the final draft for publication. The research profile of the authors can be verified from their ORCID ids, given below:

A. S. Bhosale https://orcid.org/0009-0007-1383-6383
N. P. Mali https://orcid.org/0009-0000-3018-8030
S. B. Dhotre https://orcid.org/0009-0003-3026-5181
S. P. Takle https://orcid.org/0000-0003-2966-6175
A. S. Ware https://orcid.org/0009-0000-8563-7198
D. B. Bankar https://orcid.org/0009-0004-5479-2450
R. U. Mene https://orcid.org/0000-0003-1248-4092
N. N. Bhujbal https://orcid.org/0009-0008-5778-1932

Cite this article as: A. S. Bhosale *et al.*, *Rasayan J. Chem.*, 19(3), 1482-1488(2026), https://doi.org/10.31788/RJC.2026.1939742

REFERENCES

1. X. Liu, W. Liu, Q. Tang, B. Liu, Y. Wada and H. Yang, *Earth's Future*, **10**, e2021EF002567(2022), https://doi.org/10.1029/2021EF002567
2. Y. Kharayat, Journal of Integrative Environmental Sciences, **9**, 6991(2012), https://doi.org/10.1080/1943815X.2012.688056
3. S. Netsopa, M. B. Kongkeitkajorn, P. Yuvadetkun, T. Matsuno, A. Minamino, T. Kasahara, K. Kobayashi and S. Funada, *Fuel*, **316**, 123336(2022), https://doi.org/10.1016/j.fuel.2022.123336
4. L. R. B. Silva and L. Kardos, *Journal of Environmental Geography*, **17**, 1528(2024), https://doi.org/10.14232/jengeo-2024-44674
5. P. A. Shinde, T. M. Ukarde, P. H. Pandey and H. S. Pawar, Journal of Water Process Engineering **36,** 101353(2020), https://doi.org/10.1016/j.jwpe.2020.101353
6. A. Sarma, N. Priyadarshi, R. Chakraborty and P. Kulkarni, *International Journal of Environment, Agriculture and Biotechnology,* **10**, 7685(2025), https://doi.org/10.22161/ijeab.102.8
7. M. S. Lucas, J. A. Peres and G. Li Puma, *Water*, **13**, 1309(2021), https://doi.org/10.3390/w13091309
8. S. Feijoo, X. Yu, M. Kamali, L. Appels and R. Dewil, *Reviews in Environmental Science and Bio/Technology*, **22**, 205248(2023), https://doi.org/10.1007/s11157-023-09645-4
9. R. Gautam, S. Sivakumar, I. Crasta, T. Bhaskar, S. Mudliar and D. Ghosh, Environmental Science and Pollution Research, **32,** 371382(2025), https://doi.org/10.1007/s11356-024-35779-1
10. H. Wu, L. Li, S. Wang, N. Zhu, Z. Li, L. Zhao and Y. Wang, *Physical Chemistry Chemical Physics*, **25**, 25899(2023), https://doi.org/10.1039/D3CP03391K
11. N. Goodarzi, Z. Ashrafi-Peyman, E. Khani and A. Z. Moshfegh, *Catalysts*, **13**, 1102(2023), https://doi.org/10.3390/catal13071102
12. B. S. Rasool, A. K. Abbas and R. Haddad, *Environmental Monitoring and Assessment*, **197**, 1086(2025), https://doi.org/10.1007/s10661-025-14531-3
13. R. Krakowiak, J. Musial, P. Bakun, M. Spychała, B. Czarczynska-Goslinska, D. T. Mlynarczyk, T. Koczorowski, L. Sobotta, B. Stanisz and T. Goslinski, *Applied Sciences,* **11**, 8674(2021), https://doi.org/10.3390/app11188674
14. J. Tomić and N. Malinović, *AIDASCO Review*, **1**, 2630(2023), https://doi.org/10.59783/aire.2023.27
15. A. P. Torane, A. B. Ubale, K. G. Kanade and P. K. Pagare, *Materials Today: Proceedings*, **43**, 2738(2021), https://doi.org/10.1016/j.matpr.2020.06.476
16. M. H. El-Saeid, M. O. Alotaibi, M. Alshabanat, M. M. Al-Anazy, K. R. Alharbi and A. S. Altowyan, *Water*, **13**, 655(2021), https://doi.org/10.3390/w13050655
17. T. Mao, J. Zha, Y. Hu, Q. Chen, J. Zhang and X. Luo, *Inorganics*, **12**, 178(2024), https://doi.org/10.3390/inorganics12070178
18. S. Peiris, H. B. de Silva, K. N. Ranasinghe, S. V. Bandara and I. R. Perera, *Journal of the Chinese Chemical Society*, **68**, 738769(2021), https://doi.org/10.1002/jccs.202000465
19. T. Jiang, S. Zhou, J. Yang, H. Wang, H. Yu, H. Chen, Y. Zhao, X. Yuan, W. Chu and H. Li, *Advanced Functional Materials*, **32**, 2108977(2022), https://doi.org/10.1002/adfm.202108977
20. R. Hossain, M. A. Uddin and M. A. Khan, *Journal of Physical Chemistry C*, **127**, 10897(2023), https://doi.org/10.1021/acs.jpcc.2c06981
21. S. P. Takle, O. A. Apine, D. B. Bankar, A. S. Tarlekar, N. N. Bhujbal, B. B. Kale and R. S. Sonawane, *New Journal of Chemistry*, **44**, 17724(2020), https://doi.org/10.1039/D0NJ03309J
22. W. Zhang, H. He, H. Li, L. Duan, L. Zu, Y. Zhai, W. Li, L. Wang, H. Fu and D. Zhao, *Advanced Energy Materials*, **11**, 2003303(2021), https://doi.org/10.1002/aenm.202003303
23. M. Dhaou, E. Elaloui, K. Khirouni, H. Guermazi and S. Guermazi, *Journal of Materials Science: Materials in Electronics,* **32**, 13187(2021), https://doi.org/10.1007/s10854-021-05858-x

[RJC-9742/2026]